Rare Metal Materials and Engineering
Volume 50, Issue 8, August 2021
Available online at www.rmme.ac.cn

Science Press

Cite this article as: Luo Xiao, Yang Xin, Huang Qizhong, et al. Ablation Mechanism and Properties of ZrB_2-ZrC-SiC Coating with Micro-Submicron Reinforced Structure[J]. Rare Metal Materials and Engineering, 2021, 50(08): 2678-2685.

ARTICLE

Ablation Mechanism and Properties of ZrB_2-ZrC-SiC Coating with Micro-Submicron Reinforced Structure

Luo Xiao, Yang Xin, Huang Qizhong, Su Zhean, Fang Cunqian, Chen Lei

National Key Laboratory of Science and Technology for National Defence on High-strength Structural Materials, Central South University, Changsha 410083, China

Abstract: ZrB_2-ZrC-SiC coating with micro-submicron reinforced structure was prepared on the C/C composites by vacuum infiltration and reactive melt infiltration. The micro-submicron reinforced structure consisted of micron-sized SiC as the skeleton and submicron-sized ultra-high temperature ceramic particles (UHTCs) as the filler. The ablation resistance of the composites was tested by plasma flame. Results show that during ablation, the micro-submicron reinforced structure composed of concentrated SiC particles and UHTCs is prone to form larger defects under the erosion of ablative airflow. The defects induce ablation gaps that are connected with the surrounding cracks to form larger pits, which cause part of the coating to fall off, and the failure of the whole coating system.

Key words: ceramic; micro-submicron reinforced structure coating; ablation mechanism

Carbon/carbon (C/C) composites are ideal high temperature lightweight structural materials in the aerospace field. It has the advantages of light weight, excellent high temperature performance, high thermal stability and ablative resistance[1,2]. However, due to the need for exploration and research, the C/C components of the next generation of rockets and advanced aerospace vehicles must be used as long as possible under more severe conditions[3-6]. Since carbon fibers and substrates are easily oxidized in an oxidizing environment, their oxidative ablation will cause the degradation of their physical and chemical properties, leading to the failure of composite materials at high temperatures. Therefore, additional protection is necessary to prolong the service life of the materials under harsh conditions.

To further improve ablation resistance of C/C composites at high temperature, ultra-high temperature ceramics (UHTCs) such as HfB_2, HfC, ZrB_2, ZrC and SiC have been applied on their surface or introduced into the matrix[7-10]. Among these UHTCs, researchers have paid more attention to ZrC and ZrB_2. Zirconium-based materials are a kind of abundant resources and have a lower density than other UHTCs. And the melting point of their oxides is as high as 2700 °C, which is a typical thermal barrier material and can effectively protect composites below 2500 °C[11,12]. The current methods for preparing C/C-UHTCs composite materials include chemical vapor infiltration (CVI), precursor infiltration pyrolysis (PIP), reactive melt infiltration (RMI), hot pressing sintering (HP) and some synthetic methods. In these methods, PIP and CVI processes have long preparation cycles and high cost. Due to the low ceramic yield in the PIP process, the densification course requires multiple cycles, resulting in a longer cycle and increasing labor costs and energy consumption[13]. The CVI process is relatively long and the utilization rate of source gas is low, which leads to the high cost of the final product[14]. As for preparation of UHTC coatings on C/C composites, pack cementation (PC), chemical vapor deposition (CVD) and plasma spray (PS) are the most widely used methods. All of the above methods can prepare a coating with a relatively uniform particle size and a relatively dense coating. Feng et al used two-step pack cementation method to prepare a dense coating without visible cracks, and since different phases are evenly distributed in the coating, the formation of the glass layer can effectively delay the crack and pore expansion during the ablation process[15]. Yang et al deposited a layer of HfC-ZrC-SiC coating on the SiC-coated C/C composites through plasma spraying[16]. The uniform distribution of Hf, Zr

Received date: August 25, 2020
Foundation item: Joint Funds of the National Natural Science Foundation of China (U19A2088); National Natural Science Foundation of China (51304249)
Corresponding author: Yang Xin, Ph. D., Associate Professor, National Key Laboratory of Science and Technology for National Defence on High-strength Structural Materials, Central South University, Changsha 410083, P. R. China, E-mail: yangxincsu@csu.edu.cn

and Si in the coating is beneficial to the formation of new stable phases ($HfSiO_4$ and $ZrSiO_4$), which can effectively play the role of pinning and prevent crack propagation. Wang et al deposited a uniform HfC-TaC coating on the surface of C/C composites by adjusting the process parameters of chemical vapor deposition[17]. The particle-stacked structure with uniform phase distribution makes the coating free of cracks and compact with carbon matrix. Therefore, the C/C composites can be effectively protected from ablation.

In our present study, the ZrB_2-ZrC-SiC coating with micro-submicron reinforced structure was prepared by vacuum infiltration and RMI on C/C composites. The method shows the advantages of short preparation period with low cost. More notably, the coating prepared by RMI and vacuum infiltration can form mosaic phase with micro-submicron reinforced structure, which has been less well reported. The ablative resistance of micro-submicron reinforced structure composed of heterogeneous particles is different from that of the coating structure formed by homogeneous particles. Therefore, investigation of the ablation mechanism of this micro-submicron reinforced coating structure is instructive and constructive for the design and optimization of subsequent coating structures and the improvement of their ablation resistance.

1 Experiment

The UHTC coated C/C composites were prepared by two steps: firstly, the pre-coated C/C composites were cut into several small samples and then manually polished with 600# grit SiC paper. After cleaning with anhydrous ethanol and drying in the oven, the samples were placed in a ZrB_2 powders containing slurry. The slurry was a mixture of ZrB_2 (≤0.5 μm) and ZrO_2 (≤0.5 μm) powders, and the mass ratio of ZrB_2 powder is 90wt% ~95wt% . A powder infiltration process was used to introduce the ZrB_2 particles into the C/C substrate. Subsequently, the infiltrated C/C substrate with ZrB_2 ceramic was placed around the Si powders in a graphite crucible. After a high temperature reactive melt infiltration process, the ZrB_2-ZrC-SiC UHTC coating was prepared.

The surface morphologies and crystalline structures of the coating were analyzed by scanning electron microscopy (SEM, Quanta 250 FEG, FEI, Czech) and X-ray diffraction (XRD, D/max 2550 VB, Rigaku), respectively. The thickness and width of the samples used to measure the flexural strength were 4 and 10 mm, respectively, and the fulcrum span of the measuring instrument was 40 mm. The thickness, width and height of the sample used to measure the compression strength were 6, 6 and 6.5 mm, respectively.

2 Results and Discussion

2.1 Microstructure of the micro-submicron reinforced ZrB_2-ZrC-SiC coating

Fig. 1 shows the BSE image and SEM morphology of the porous C/C preform infiltrated with ceramic particles. From Fig. 1a, some pores can be clearly found, and the existence of these pores can effectively promote the next step of silicon infiltration. From Fig. 1b, the black phases are carbon fibers and pyrolytic carbon, and the white phases are ZrB_2. The existence of white phase proves that the powders can be effectively infiltrated into the carbon substrate by vacuum infiltration. According to Fig. 1a and Fig. 1b, the ceramic particles are mainly concentrated in fiber bundles with pores around tens of micrometers.

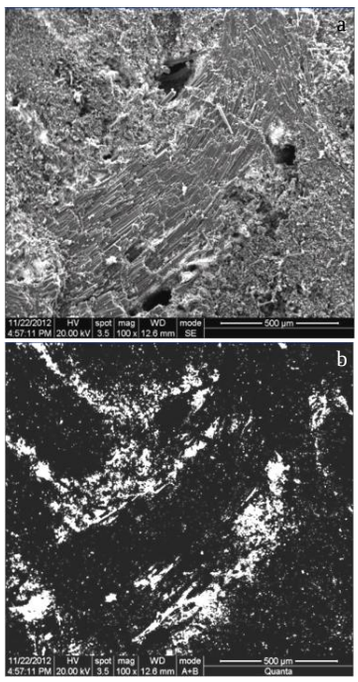

Fig.1 SEM morphology (a) and corresponding BSE image (b) of the porous C/C preform infiltrated with ceramic particles after the powder infiltration process

Fig. 2 shows the XRD results of ZrB_2-ZrC-SiC coating. According to the analysis, ZrB_2, ZrC and SiC are the main phases of the ZrB_2-ZrC-SiC coating. The surface morphologies of the ZrB_2-ZrC-SiC coating are shown in Fig. 3. From Fig. 3a, the phases are stacked to form a relatively dense coating, and some white phases are distributed evenly in the coating. As shown in Fig. 3b, fewer pores are found on the coating surface, because the pores are effectively filled by UHTCs after reactive melt infiltration process. Through EDS analysis, it can be found that micrometer-sized particles are SiC and submicron particles are UHTCs. The main reason for the difference in size is that SiC grains grow faster than UHTCs.

Fig. 4 shows SEM images and EDS result of the ZrB_2-ZrC-SiC coating. As shown in Fig. 4a, owing to the lack of transition layer and the weak bonding ability between ceramic coating and substrate, larger gaps can be observed at the interface. Fig. 4b shows that the large SiC particles are embedded with many submicron-sized UHTC particles, forming a compact mosaic stacking structure. This structure is further confirmed by the cross-section of Fig. 4a. It can be

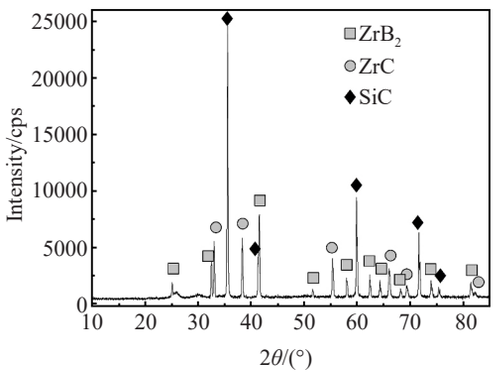

Fig.2 XRD pattern of prepared ZrB_2-ZrC-SiC coating on C/C composites

found that the SiC particles generated in the process of the silicon infiltration fills the pores in the UHTC particles, thus forming the micro-submicro reinforced structure. Fig. 4c displays the EDS element line scanning of ceramic coating, and the thickness of ZrB_2-ZrC-SiC coating is about 200 μm. The outer layer of the ceramic coating is mainly made of micron-sized SiC, and the submicron-sized Zr-based UHTC phases mainly aggregate in the inner layer close to the matrix.

2.2 Microstructure of ZrB_2-ZrC-SiC coated C/C composites

Fig. 5 shows the XRD results of the ZrB_2-ZrC-SiC coated C/C composites, which indicates that ZrB_2, ZrC and SiC ceramics are formed in the system under the established process. The phase of ZrB_2, ZrC and SiC are generated by the infiltrated ZrB_2 powders, reaction of ZrO_2, and Si powders with PyC, respectively.

Fig. 6 displays the SEM micrographs of the ZrB_2-ZrC-SiC coated C/C composites. After vacuum impregnation and RMI process, small ceramic particles can be found between fiber bundles. From Fig. 6a, micron-submicron particles are clearly observed in the figure, indicating that the powders are

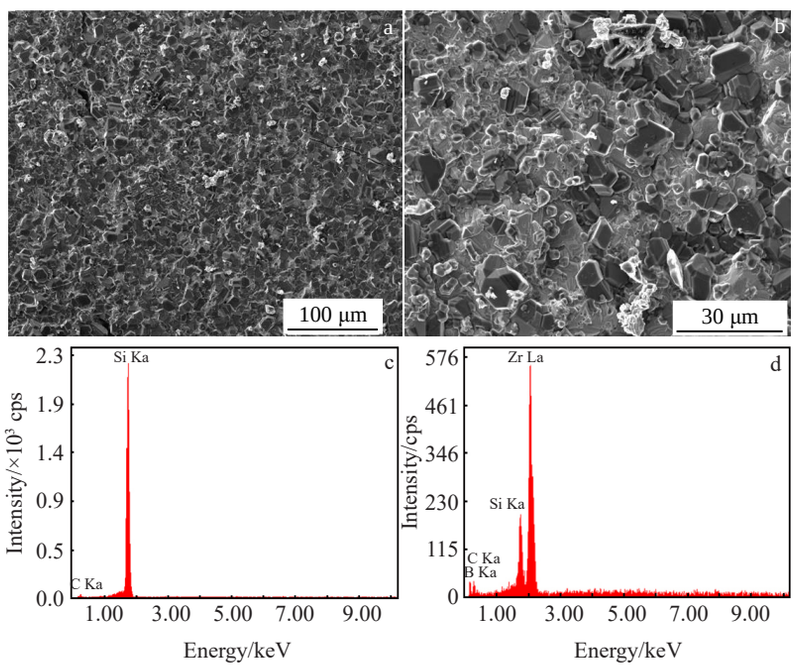

Fig.3 SEM images of surface morphologies (a, b) and EDS spectra (c, d) of the ZrB_2-ZrC-SiC coating on C/C composites

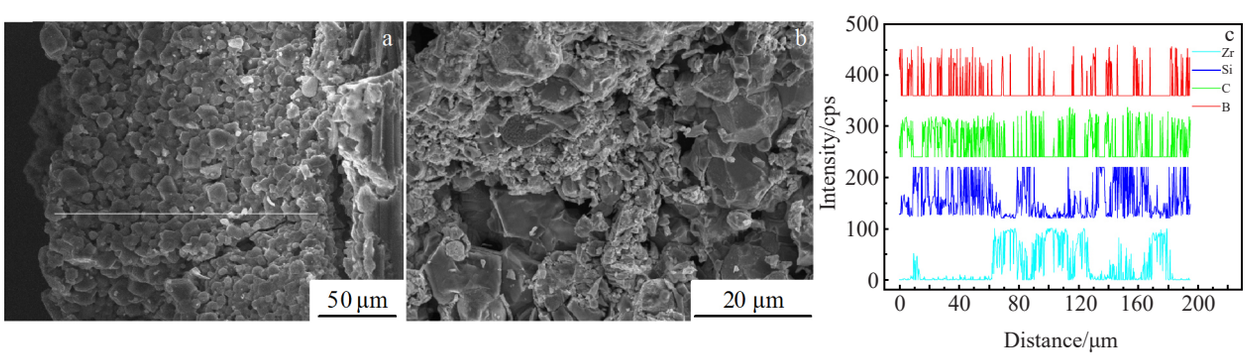

Fig.4 SEM images of cross-section of the coating (a) and ZrB_2-ZrC phases in the coating (b); EDS line scanning of the ZrB_2-ZrC-SiC coating (c)

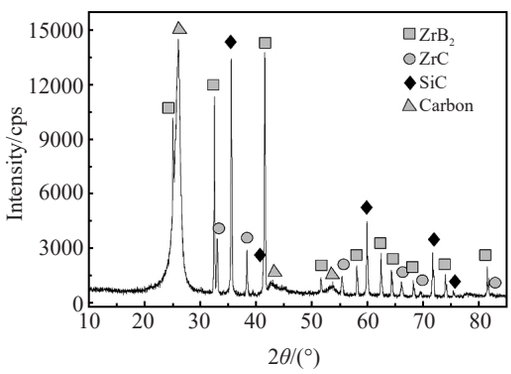

Fig.5 XRD pattern of ZrB_2-ZrC-SiC coated C/C composites prepared by powder infiltration and RMI process

effectively infiltrated into the carbon matrix in the established process. According to the Fig. 6b and 6c, the ZrC-SiC ceramics are filled between the fibers of the carbon matrix, effectively filling some of the pores in the matrix. The good wetting properties of silicon and PyC allow Si to infiltrate into the substrate well. Fig. 6d is a microscopic topography of the ceramic particles in the matrix, which is similar to the coating. It can be seen that SiC particles and UHTCs are uniformly distributed in the substrate. The size of the SiC particles in the matrix is several micrometers to several tens of micrometers, which is smaller than the size of formed SiC crystals in the coating. Meanwhile, the UHTC particles reveal submicron scale in the matrix.

2.3 Mechanical properties of the ZrB_2-ZrC-SiC coated C/C composites

Fig. 7 shows the fracture surface micrographs of the ZrB_2-ZrC-SiC coated C/C composites. The macroscopic fracture is uneven, including pulling out of fiber bundle, cracking of matrix and delamination of fiber layer. Fig. 7b shows the fracture, from which it is obvious that a large amount of carbon fiber is pulled out, which can produce new surfaces that absorb more energy, thus improving fracture toughness.

The mechanical properties of the ZrB_2-ZrC-SiC coated C/C composites were evaluated by the flexural and compression test. Fig. 8 displays the typical flexural load-displacement curves of the ZrB_2-ZrC-SiC coated C/C composites. And Table 1 shows that the average bending and compression strength of the composites are 134.13 and 97.11 MPa, respectively. Fig. 9 displays the compressive load-displacement curves of the ZrB_2-ZrC-SiC coated C/C composites.

All the curves reveal the same characteristics: the load increases linearly before it reaches the maximum value. Once the maximum load is passed, the curve descends in a stepped manner, which indicates that all the four samples have a certain degree of pseudo-plastic fracture behavior.

2.4 Ablation resistance of micro-submicron reinforced ZrB_2-ZrC-SiC coating under the plasma flam

The ablation resistance of multiphase enhanced coatings was studied by plasma flame ablation test. After 60 s of ablation, the linear and mass ablation rates of the ZrB_2-ZrC-

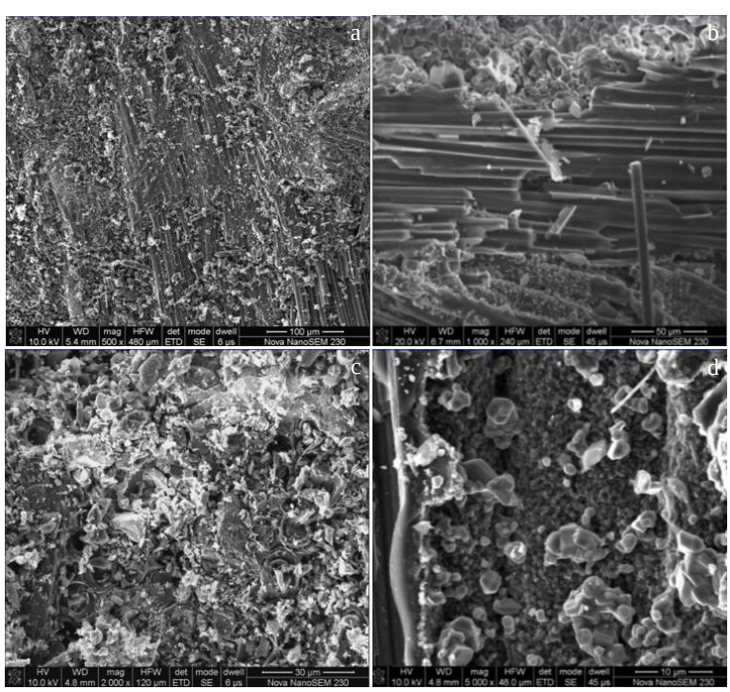

Fig.6 SEM micrographs of the ZrB_2-ZrC-SiC coated C/C composites: (a) cross-section of the C/C-ZrC-SiC composites, (b) ZrC-SiC ceramics formed between non-woven fiber cloth and short-cut-fiber web layers, (c) ZrC-SiC ceramics filling pores between carbon fibers, and (d) magnified morphology of ZrC-SiC ceramics

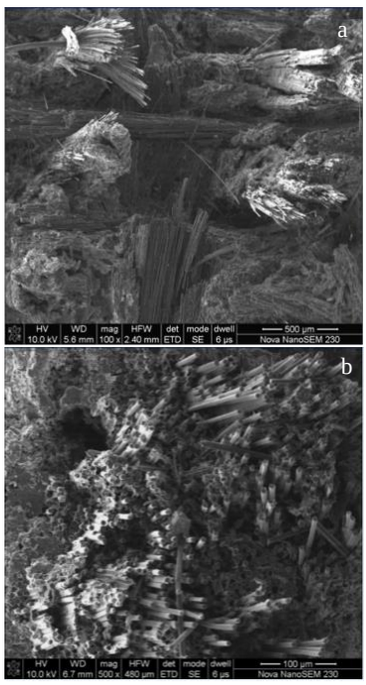

Fig.7 Fracture surface micrographs of the ZrB_2-ZrC-SiC coated C/C composites after flexural test: (a) fracture surface and (b) pulled-out carbon fibers

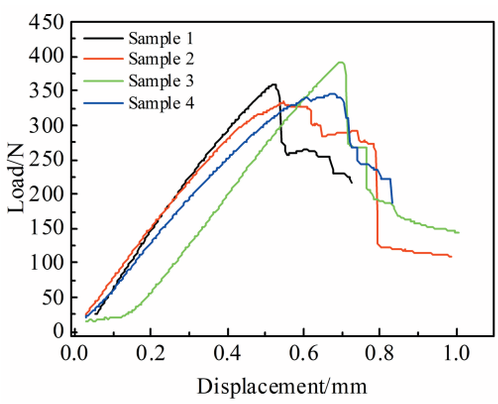

Fig.8 Typical flexural load-displacement curves of the coated C/C-ZrB_2-ZrC-SiC composites

SiC coated C/C composites are 8.42 μm/s and 0.7 mg/s, respectively. These results suggest that C/C composites with ZrB_2-ZrC-SiC coating have good ablation resistance.

Fig. 10 shows macrograph of the ZrB_2-ZrC-SiC ceramic coating after ablation for 60 s. The center of the coating is peeled off, causing the coating to fail. The main reason for the coating failure is the lack of transition layer, so a serious thermal expansion coefficient mismatch occurs between the coating and matrix. Further reasons for coating failure will be discussed in the ablation mechanism section. From Fig.11a to Fig.11d, under the peeled-off ZrB_2-ZrC-SiC coating, a layer of fine UHTC particles is present in the ablation center, and

Table 1 Bending strength and compression strength of the ZrB_2-ZrC-SiC coated C/C composites

Sample	Bending strength/MPa	Compression strength/MPa
1	134.86	99.60
2	125.12	95.38
3	146.57	95.36
4	129.96	98.08
Average	134.13	97.11

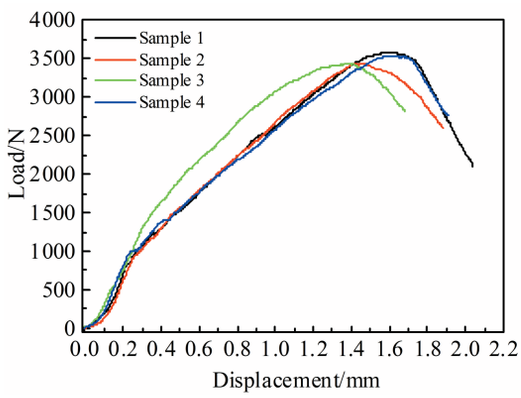

Fig.9 Compressive load-displacement curves of the ZrB_2-ZrC-SiC coated C/C composites

fewer larger SiC particles can be seen. ZrB_2 particles are gathered on the C/C substrate by the powder infiltration process. During the later RMI process, some ZrO_2 particles react with carbon to generate ZrC and concentrate in the matrix, and others are gathered on the surface of the matrix.

2.5 Ablation mechanism

In the plasma flame ablation test, the reactions below may occur:

$2ZrB_2\ (s) + 5O_2\ (g) \rightarrow 2ZrO_2\ (s) + 2B_2O_3\ (l)$

$B_2O_3(l) \rightarrow B_2O_3(g)$

$ZrB_2(s) + 5H_2O(g) \rightarrow ZrO_2(s) + B_2O_3(g) + 5H_2(g)$

$ZrC\ (s) + 2O_2\ (g) \rightarrow ZrO_2\ (s) + CO_2\ (g)$

$ZrC\ (s) + 3H_2O\ (g) \rightarrow ZrO_2\ (s) + CO\ (g) + 3H_2(g)$

$SiC\ (s) + 2O_2\ (g) \rightarrow SiO_2\ (l) + CO_2\ (g)$

$SiC\ (s) + 3H_2O\ (g) \rightarrow SiO_2\ (l) + CO\ (g) + 3H_2(g)$

$SiO_2\ (l) \rightarrow SiO_2\ (g)$

The ZrB_2-ZrC-SiC coating reacts with oxidizing gases (O_2 and H_2O) to form ZrO_2 and SiO_2 products on the ablated surface, with emitting of CO and CO_2 gases. According to the previous research[18], the boron oxide generated in the ablation process can evaporate rapidly, slowing down the temperature increase of the coating surface. In addition, with the increase of temperature and erosion force, the formed SiO_2 inside the coating cannot withstand erosion and begins to soften and fall apart, and a large amount of SiO_2 evaporates. The failure of the coating can be analyzed from the following levels. Firstly, due to the lack of transition layer in the coating system, a serious thermal expansion coefficient mismatch between the coating and the carbon matrix can cause thermal stress

Fig.10 Macrograph of the ZrB_2-ZrC-SiC coated C/C composites after ablation under the plasma flame for 60 s

concentration, leading to the formation of cracks and cracking of the coating. Secondly, the formed cracks and the pores in the coating can provide diffusion channels for ablative gas to attack the substrate, so the interface is further oxidized and damaged, degrading the bonding ability of the coating. Meanwhile, the proliferation and propagation of the cracks will accelerate the evolution of defect formation. Thirdly, as the ablation process prolongs, the consumption of SiO_2 scales along the grain boundary can generate ablation gaps between the grains, resulting in the weakened bonding force of grains to resist the scouring of strong airflow. Therefore, with the increased ablation gaps and decreased bonding ability between grain boundaries, the small particles in the reinforced coating lose the support of the large grains and most of them go away with the strong scouring air, causing the coating to collapse.

The ablation mechanism can be summarized as follows. In the early stage of ablation, cracks occur in the coating due to thermal stress, causing partial UHTC particles on the coating to peel off. The large SiC particles exposed to the ablative airflow are directly scoured, and the interface between the large particles (SiC grains) is first oxidized to form a thin SiO_2 layer on SiC particles (Fig. 12b). However, the SiO_2 molten layer cannot withstand the high temperature airflow, which results in the outer SiO_2 layer and the adhered ZrO_2 small particles to be scoured away by the ablative airflow (Fig.12c). As the interparticle interface is further oxidized, the gaps between the interfaces become larger, resulting in insufficient bonding force between the particles. Under the strong scouring effect of the airflow, the large SiC particles are peeled off, forming a corresponding ablation pit. Then, the ablation pit is connected with the surrounding microcracks, causing the small UHTCs embedded around the remaining large SiC particles to lose their support and peel off (Fig.12d). At the same time, the cracks around the pits may become the oxygen diffusion channel, which can also generate ablation pores around the inner particles. As the ablative airflow reaches the inside of the coating along the pores, the coating begins to oxidize from the inside; therefore, the oxidized SiC skeleton begins to soften, and part of the silica products convert to the liquid phase, resulting in poor strength and scouring resistance, which cannot play the role of skeleton

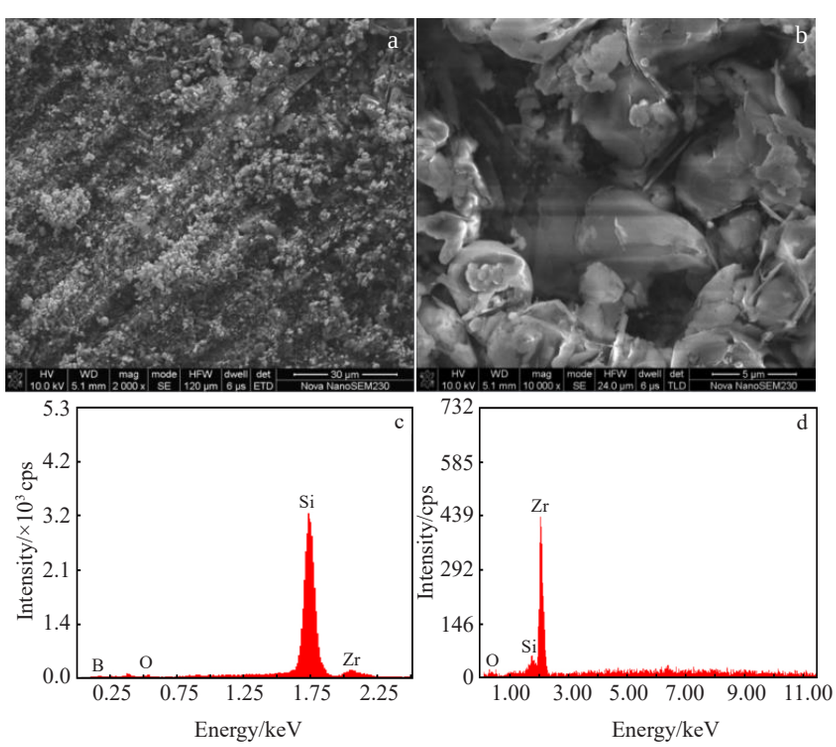

Fig.11 Surface images of the ZrB_2-ZrC-SiC coated C/C composites after ablation under the plasma flame for 60 s: (a) composites under the peeled-off ZrB_2-ZrC-SiC coating and (b) ceramic products on the composites surface; (c, d) EDS spectra of the ablated molten products

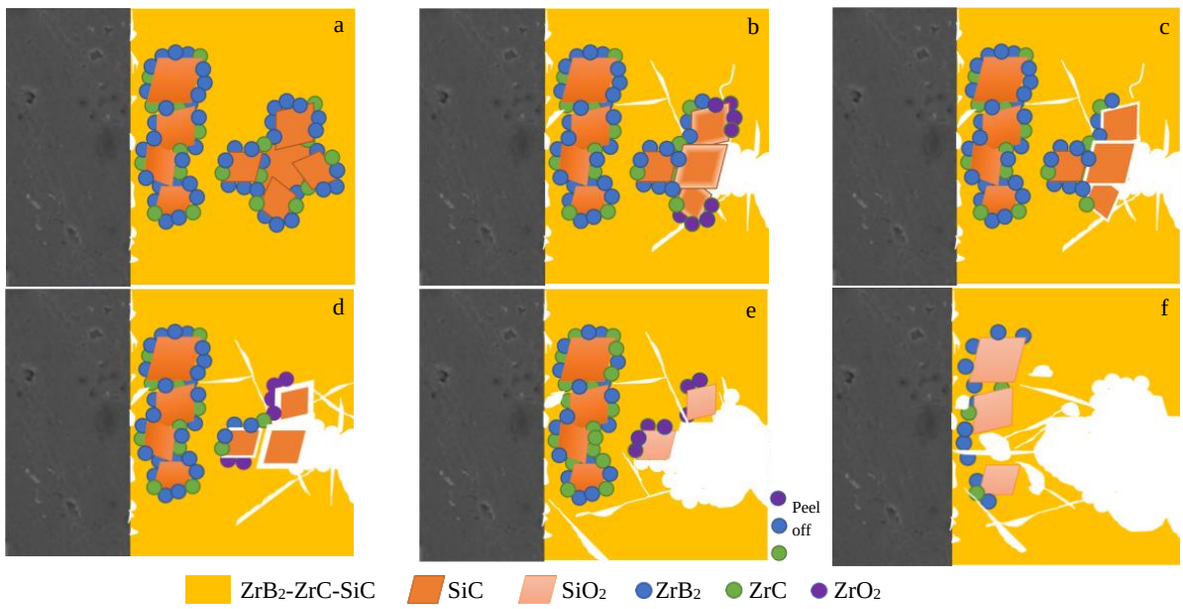

Fig.12 Ablation schematic diagram of the ZrB_2-ZrC-SiC coated C/C composites: (a) before ablation, (b) initial stage of ablation, (c, d) middle stage of ablation, and (e, f) final stage of ablation

strengthening (Fig. 12e). Zirconium carbide and zirconium boride are oxidized to form zirconia. Zirconia originally has good effect on improving the viscosity of the liquid phase, but the content is too low so that it can be easily blown away (Fig. 12f). In this case, the zirconia cannot form continuous skeleton and the severe softening and ablation of the SiC skeleton induce the failure of the coating. Therefore, the failure of the ZrB_2-ZrC-SiC coating with micro-submicron reinforced structure can be attributed to the high content of SiC skeleton and low content of UHTC phases in the coating system.

3 Conclusions

1) The ZrB_2-ZrC-SiC coating reinforced with micro-submicron grains can be prepared by vacuum infiltration and reactive melt infiltration. The micron-sized SiC particles form the skeleton of the coating, with the surrounding submicron-sized UHTC particles as the filler. UHTCs are embedded around the SiC particles to form the micro-submicron reinforced structure with mosaic phase. After ablation for 60 s, and the linear and mass ablation rates of the composites are 8.42 μm/s and 0.7 mg/s, respectively.

2) The major reasons for the coating failure are the lack of transition layer and high content of SiC skeleton. During ablation, the lack of transition layer induces cracks in the coating. Meanwhile, ablation gaps are formed along grain boundaries. Under the strong scouring effect, the increased ablation gaps and decreased bonding ability between grain boundaries result in the peeling off of small particles, generating a ablation pit in the ablation center. Due to the high content of SiC skeleton and low content of UHTC phases in the coating, the zirconia cannot form continuous skeleton and the severe softening and ablation of the SiC skeleton cause the failure of the coating.

References

1 Zaman Wajed, Li Kezhi *et al. Corrosion Science*[J], 2012, 61: 134
2 Zhu Yulin, Wang Song, Li Wei *et al. Rare Metal Materials and Engineering*[J], 2013, 42(S1): 447 (in Chinese)
3 Paul A, Jayaseelan D, Venugopal S *et al. American Ceramic Society Bulletin*[J], 2012, 91(1): 22
4 Sziroczak D, Smith H. *Progress in Aerospace Sciences*[J], 2016, 84: 1
5 Bianchi Daniele, Nasuti Francesco, Martelli Emanuele. *Journal of Spacecraft and Rockets*[J], 2009, 46(3): 492
6 Thakre Piyush, Yang Vigor. *Journal of Propulsion and Power*[J], 2008, 24(4): 822
7 Jin Xiaochao, Fan Xueling, Lu Chunsheng *et al. Journal of the European Ceramic Society*[J], 2018, 38(1): 1
8 Tang Sufang, Hu Chenlong. *Journal of Materials Science & Technology*[J], 2017, 33(2): 117
9 Opeka Mark M, Talmy Innna G, Wuchinaa Eric J *et al. Journal of the European Ceramic Society*[J], 1999, 19(13-14): 2405
10 Fahrenholtz William G, Hilmas Gregory E, Talmy Inna G. *Journal of the American Ceramic Society*[J], 2007, 90(5): 1347
11 Hu Ping, Wang Guolin, Wang Zhi. *Corrosion Science*[J], 2009, 51(11): 2724
12 Wen Bo, Ma Zhuang, Liu Yanbo *et al. Rare Metal Materials and Engineering*[J], 2015, 44(11): 2782 (in Chinese)
13 Langlais F. *Comprehensive Composite Materials*[J], 2000, 4: 611

14 Xie Changming, Chen Mingwei *et al. Journal of the American Ceramic Society*[J], 2012, 95(3): 866
15 Feng Tao, Li Hejun, Hu Manhong *et al. Journal of Alloys and Compounds*[J], 2016, 662: 302
16 Yang Yang, Li Kezhi, Zhao Zhigang *et al. Ceramics International*[J], 2017, 43(1): 1495
17 Wang Yalei, Xiong Xiang, Li Guodong *et al. Corrosion Science* [J], 2013, 66: 177
18 Huang Dong, Zhang Mingyu, Huang Qizhong *et al. Corrosion Science*[J], 2015, 98: 551

具有微米-亚微米增强结构的ZrB_2-ZrC-SiC涂层的烧蚀机理与性能

罗　骁，杨　鑫，黄启忠，苏哲安，方存谦，陈　蕾
(中南大学 轻质高强结构材料国防科技重点实验室，湖南 长沙 410083)

摘　要：通过真空浸渗和反应熔渗在C/C复合材料上制备了具有微米-亚微米增强结构的ZrB_2-ZrC-SiC涂层。微米-亚微米增强结构由微米级的碳化硅为骨架，亚微米级的超高温陶瓷颗粒（UHTCs）为填充料组成。采用等离子火焰对复合材料进行了烧蚀试验。结果表明，在烧蚀过程中由聚集的碳化硅颗粒和超高温陶瓷颗粒组成的微米-亚微米增强结构在烧蚀气流的侵蚀下易于形成较大的缺陷。已形成的较大缺陷容易与缺陷周围的裂纹相连形成较大的凹坑，从而导致部分涂层脱落，并导致整个涂层系统失效。

关键词：陶瓷；微米-亚微米增强结构涂层；烧蚀机理

作者简介：罗　骁，男，1996年生，硕士，中南大学轻质高强结构材料国防科技重点实验室，湖南 长沙 410083，E-mail：13787416236@163.com